



Numerical Simulation of Flow behind Vortex Generators

N. K. Singh

Department of Mechanical Engineering, National Institute of Technology, Kurukshetra, Haryana, 136119, India

†Corresponding Author Email: nksinghfme@nitkr.ac.in

(Received July 2, 2018; accepted October 23, 2018)

ABSTRACT

In this study, flow behind rectangular vane type vortex generators mounted on a flat plate, is numerically simulated using the immersed boundary (IB) method. In the present work, the direct forcing IB method is employed because of its simplicity and high efficiency. Vortex generators of two different heights are numerically investigated. The height of vanes in the first case is close to the definition of submerged/low-profile vortex generators while the other case is closer to the definition of a conventional vortex generator. The resultant highly three-dimensional flow and its transition to turbulence have been studied. Counter-rotating vortices generated by these passive rectangular vortex generators are characterized. Streamwise evolution of non-dimensionalised maximum values of vorticity, vortex strength, streamwise velocity and wall-normal velocity are studied. The simulations show that the IB method in conjunction with DNS effectively simulates the time-dependent flow behind an array of passive vortex generators placed in an initially laminar boundary layer.

Keywords: Rectangular vortex generators; Direct numerical simulation; Immersed boundary method.

NOMENCLATURE

C_f	skin friction coefficient	u_m	mean streamwise velocity
C_p	coefficient of pressure	U_∞	free stream velocity at inlet
D	spanwise spacing between VGs	τ_w	wall shear stress
d	spanwise blade spacing within VG	δ	boundary layer thickness
h	VG blade height	δ^*	displacement thickness
p	pressure	δ_m^*	displacement thickness at inlet
$Re_{\delta_m^*}$	Reynolds number based on displacement thickness at inlet and free stream velocity	θ	momentum thickness
rms	root mean square	θ_s	momentum thickness at separation
u_τ	friction velocity		

1. INTRODUCTION

A phenomenal increase in computer memory as well as computing speed has led to a huge surge in CFD capability. The field of flow separation control too, which relies heavily on empiricism, has not remained untouched. Of late, there have been several efforts to complement experimental work with CFD data. However, numerical simulation of flow behind a vortex generator is still considered difficult as the computational domain has to include

both the vortex generator as well as the target area downstream where control is desired. As the size of the vortex generator is rather small compared to the full computational domain, full resolution of the boundary layers of the vortex generator as well as the mounting surface (e.g. airfoil or flat plate) would be computationally prohibitive.

The height of conventional, passive vortex generators (VGs), h , is of the order of boundary layer thickness, δ . Such VGs have been in use since 1940s (Taylor, 1948a). These simple and

effective devices consist of vanes of different shapes attached to the mounting surface. The vanes are usually placed at an angle to the oncoming flow. They generate embedded longitudinal vortices to transfer momentum to near-wall flow making use of micro-movements (Gad-el-Hak and Bushnell, 1991a). In the vortices, fluid with high streamwise momentum moves helically to mix with the slow-moving near-wall flow and replace it. Passive vortex generators have been applied to compressor blades, diffusers (Brown *et al.*, 1968) and airfoils (Pearcey, 1961; Bragg and Gregorek, 1987) etc. Research, both basic fluid-dynamic and applied, has been mainly experimental in nature and numerical simulations started appearing in the past decade only. Guidelines for conventional vortex generators can be found in papers by Taylor (1948b), Henry *et al.* (1956) and Pearcey (1961). Inviscid theory was applied by Pearcey (1961) to predict the cross-stream movement of vortices as they travel downstream. He also prescribed the optimum ratio for spanwise spacing (D) to spanwise blade spacing within the pair (d) as $D/d \approx 4$ and the ratio of spanwise spacing to blade height (h) as $D/h \approx 10$.

The conventional vortex generators have been used in varied forms, in the form of rectangular vanes, triangular vanes, backward or forward ramp, wishbones and doublets etc. Though rugged and low-cost, these devices produce considerable parasitic drag and the recent trend is to reduce the device height from $O(\delta)$ to $O(\delta/5)$ or less. This reduction in height significantly reduces the parasitic drag. It is made possible because of availability of required momentum levels close to the surface (Lin and Howard, 1989; Lin *et al.*, 1990; Gad-el-Hak and Bushnell, 1991b; Lin, 2002). However, the sub-boundary layer devices need to be placed relatively closer to the separation location and these are more suitable where the flow-separation line does not change its position appreciably. Wind tunnel tests were conducted by Kerho *et al.* (1993) to assess the performance of various types of submerged vortex generators in controlling the laminar separation bubble present on a low Reynolds number LA2573A airfoil. The Reynolds numbers ranged from 200,000 to 600,000 and the angles of attack were less than the stall angle. An analytical study of three-dimensional turbulent flow triggered in a boundary layer by vortex generators mounted on the surface was carried out by Smith (1994). Analytical formulae were suggested by him for favourable vortex generator distributions.

Bender *et al.* (1999) used a new approach to model a vortex generator vane. In their analysis, they introduced a source term representing the side force produced by vanes. The strength of this source term depends on the local flow. Hamstra *et al.* (2000) used the simplified model of VG vane given by Bender *et al.* (1999) to compare their simulation of vortex generator vanes with experimental results. Allan *et al.* (2002) numerically simulated a single VG vane and a vortex generating jet for flow over a flat plate. The height of the VG vane was just a

fraction of the boundary layer thickness. Their computations involved the steady-state solution to the Reynolds-averaged Navier-Stokes equations. However, their simulations underestimated the initial magnitude of peak streamwise vorticity and its decay was poorly predicted. A more diffused vortex was generated by the numerical simulations. However, the vortex strength matched well with the experimental observations. A comprehensive review on deployment of low-profile vortex-generators can be found in Lin (2002).

Sohankar and Davidson (2003) performed direct numerical simulation and large-eddy simulations for resolutions up to 1.2 million points to examine the effect of vortex generators on the flow-field and heat transfer in a plate-fin heat-exchanger. Godard and Stanislas (2006) performed a detailed experimental study for optimization and characterization of passive vortex generators. They tabulated the optimal configuration for both co-rotating and counter-rotating devices and concluded that counter-rotating devices are more effective than the co-rotating ones. Shan (2007) used the immersed boundary method in conjunction with DNS to investigate the flow-field behind a pair of active vortex generators on a flat plate. Shan *et al.* (2008) numerically simulated subsonic flow separation over a NACA0012 airfoil. They investigated control of flow separation using both passive and active vortex generators. It was observed by them that the separation zone was completely eliminated by active vortex generators separation while the use of passive vortex generators led to a reduction in the averaged separation zone by more than 80%. Henze *et al.* (2011) have created a benchmark data set for flow-field and heat transfer characteristics in the presence of longitudinal vortices for a Reynolds number of 300,000. A number of investigations on different geometries of vortex generators, both experimental and numerical, have been carried out by Velte *et al.* (2007, 2013, 2014) to study vortex generator induced flow field and its effect on separation control.

In the present work, the immersed boundary method has been combined with DNS in Cartesian coordinates to resolve the flow-field behind rectangular vortex generators. The VG blades are mounted perpendicular to the flat plate with an angle of 30° to the incoming flow. The blades are $4\delta_{in}^*$ (32 mm) long and $0.4\delta_{in}^*$ (3.2 mm) thick. The center-to-center blade spacing (d) is $5\delta_{in}^*$ while the distance between two VG pairs (D) is $15\delta_{in}^*$. Vortex generators of two heights have been investigated, $h = 1\delta_{in}^*$ and $h = 2\delta_{in}^*$. The counter-rotating vortices generated are characterized, while streamwise evolutions of non-dimensionalised maximum values of vorticity, vortex strength, wall-normal velocity and spanwise velocity are presented. One of the objectives of the work is to resolve the three-dimensional flow structures and correlate with turbulence evolved due to the vortex generators.

2. NUMERICAL FORMULATION

2.1 Governing Equations

The incompressible mass and momentum equations are solved which can be given as,

$$\frac{\partial u_j}{\partial x_j} = 0 \quad (1)$$

and

$$\frac{\partial u_i}{\partial t} + \frac{\partial}{\partial x_j} (u_j u_i) = -\frac{\partial p}{\partial x_i} + \frac{1}{\text{Re}_{\delta_{in}^*}} \nabla^2 u_i + F_i \quad (2)$$

where, u_i represents the velocity field and $\text{Re}_{\delta_{in}^*}$ is the Reynolds number based on displacement boundary layer thickness δ_{in}^* and the inlet free stream velocity U_c . The presence of the body forces F_i is due to the immersed boundary method (Muldoon & Acharya, 2005).

2.2 Computational Details

The dimensions of the computational domain are the same as in previous simulation of laminar separation bubble (Singh and Sarkar, 2011) i.e., $L = 200 \delta_{in}^*$, $W = 30 \delta_{in}^*$, $H = 10 \delta_{in}^*$. This has been done considering the future goal of control of separation using the vortex generators. The placement of vortex generators in the domain is shown schematically in Fig. 1.

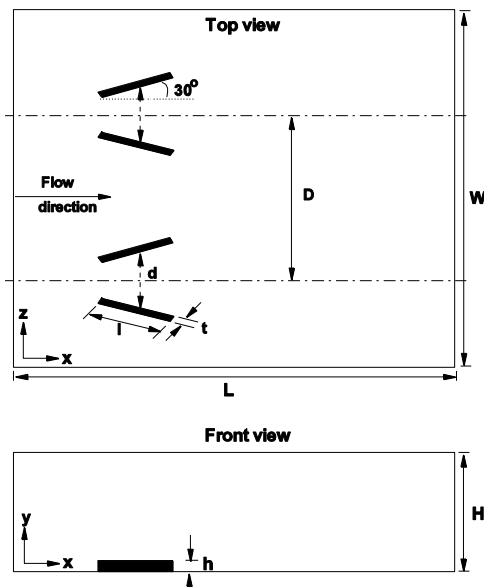


Fig. 1. Schematic of computational domain showing the placement of vortex generators (not to scale).

The dimensions of the vortex generators have been chosen to lie within the parameters laid down by Pearcey (1961) and Lin (2002) for producing long-

lasting vortices. The blade length (l) is $4 \delta_{in}^*$ for both the cases. The vortex generator thickness (t) has been taken as $0.1l$ while the vortex generator height is $1.0 \delta_{in}^*$ in the first case, denoted as *VG-1* and $2.0 \delta_{in}^*$ in the second case, denoted as *VG-2*. The distance between vortex blades at the mid-section (d) is $5.0 \delta_{in}^*$, while the distance between two vortex generator pairs (D) is $15 \delta_{in}^*$. Two pairs of rectangular VG blades have been placed in the laminar region, upstream of the location, where the flow separates in the uncontrolled case, the trailing edge being at $x = 10.64 \delta_{in}^*$. They have been arranged to generate counter-rotating vortices. It was shown by Godard and Stanislas (2006) that vortex generators generating counter-rotating vortices are more efficient than co-rotating ones by a factor of two. For the present study δ_{in}^* is calculated as 8 mm while the boundary-layer thickness at the location of vortex generators is 24 mm implying that both the vortex generators have sub-boundary layer heights. The boundary conditions used at inlet, outlet, in flow normal direction and spanwise direction are discussed below.

At the inlet, a Blasius velocity profile is specified for the streamwise velocity component corresponding to $\text{Re}_{\delta_{in}^*} = 500$, the wall normal and the spanwise velocity components are set to zero. At the outlet, a non-reflective boundary condition (Orlanski, 1976) is imposed which can be written as

$$\frac{\partial u_i}{\partial t} + U_c \frac{\partial u_i}{\partial x_c} = 0 \quad (3)$$

Here, subscript c denotes the direction normal to the outflow boundary. The convective velocity (U_c) is considered as constant across the outflow boundary and is fixed at each time step by averaging the velocity normal to the boundary over a transverse plane.

On the lower boundary a no-slip condition is applied i.e. $u = v = w = 0$. At the upper boundary, a Dirichlet boundary condition is applied to the stream wise velocity component ($u = 1.0$) and the other two components are set to zero (i. e. $v = w = 0.0$). A periodic boundary condition is applied to all the velocity components in the spanwise direction, while the no-slip velocity condition ($u = v = w = 0$) is imposed on the vortex generator surfaces using the immersed boundary method.

The solver used here has been validated in previous studies (Sarkar and Sarkar, 2009) on transitional and turbulent flows. The computational domain is divided into $356 \times 128 \times 128$ cells along x , y and z directions respectively. Fig. 2 shows the grid-resolutions along the wall.

Along spanwise direction uniform grid-spacing has been used while in the other two directions the

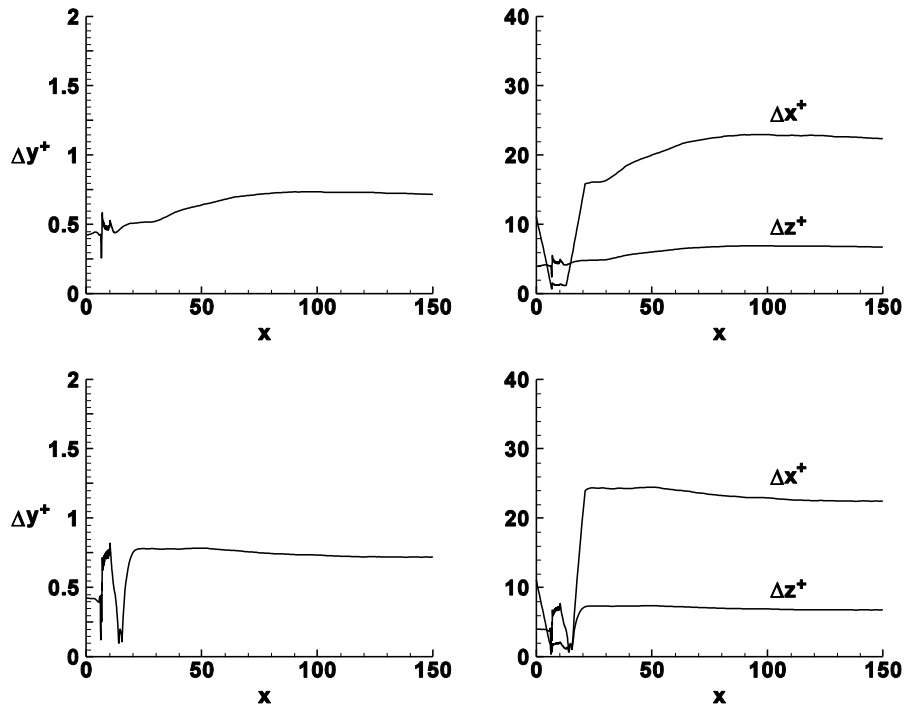


Fig. 2. Near wall grid resolutions in wall units for (a) case *VG-1* and (b) case *VG-2*.

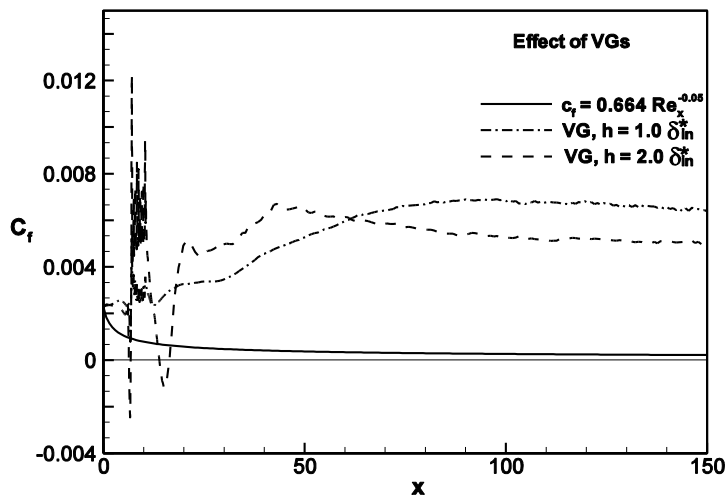


Fig. 3. Variation of mean skin friction coefficient. The Blasius C_f profile is also superimposed.

grid-spacing is non-uniform. Δy^+ for the wall-nearest grid-point remains around 0.6, indicating a well-resolved viscous sub-layer. Near the vortex-generators, a very fine grid has been used to resolve the vortex generator boundary layer, Δx^+ in this zone being around 1.2 wall units. The value of Δz^+ remains around 6 wall units.

The time-step Δt for solution advancement is 0.02 in dimensionless units. Around 10000 iterations are needed for one flow pass. Initially, seven flow passes with wall disturbances are allowed for the evolution of flow. Statistics are taken for further ten flow passes after the flow reaches dynamic stability. The simulation took about 700 hrs on an Intel Xeon, 2.6 GHz, quad-core, twin processor machine with

16 GB RAM.

3. RESULTS AND DISCUSSION

Numerical simulations of vortex generators on a flat plate have been performed for two different device heights, $1 \delta_{in}^*$ (8 mm) and $2 \delta_{in}^*$ (16 mm) and compared with available experimental results. The flow is analysed by time-averaged and instantaneous data apart from spectral study. Further, characterization of the vortex generators is carried out by figuring out the path of the streamwise vortex core, decay of the peak vorticity and the vortex strength.

3.1 Mean Flow Characteristics

In this section, the time-averaged results are presented where the data are also space averaged. This has been done to visualize the effect of VG in distorting boundary layer and its downstream development. Thus to illustrate further all the results are presented, where growth of the Blasius layer is superimposed. In reality, the flow is highly anisotropic in the spanwise direction. Therefore, in the next section, the time-averaged results are presented, which are the function of three directions.

3.1.1 Mean Skin Friction Coefficient

Figure 3 shows the evolution of C_f for different VG heights. The flow is highly distorted due to warping of the boundary layer around the VG developing two counter-rotating vortices that convect downstream. Sometimes, a tiny separation bubble is observed just downstream of VG. The plot of C_f gives information about the mean bubble length. No separation is seen in the case of smaller height vortex generator (*VG-1*) while the presence of vortex generators of greater height (*VG-2*) induces the formation of a short separation bubble. The separation and reattachment points of the bubble in the case *VG-2*, evaluated by the zero crossings of the C_f plot, are 13.9 and 16.4 respectively implying a bubble length of 2.5. Further, the presence of a very tiny mean bubble of length 0.5 is seen close to the leading edge of the vortex generator. As the flow relaxes downstream of $x = 50$, the C_f is considerably higher than that of Blasius layer. It appears that flow becomes rapidly turbulent downstream of VG.

3.1.2 Coefficient of Pressure

The variation of normalized wall pressure ($-C_p$) for different VG heights is depicted in Fig. 4. The presence of vortex generators creates a region of favourable pressure gradient; the pressure drop being steeper in the case *VG-2*. At the end of vortex generator region, a sudden pressure rise follows, the rise being severe enough in the case *VG-2* to cause separation. The separation bubble formed in this case is located in the region of strongest adverse pressure gradient. A slow favorable pressure gradient is observed downstream indicating relaxation of boundary layer.

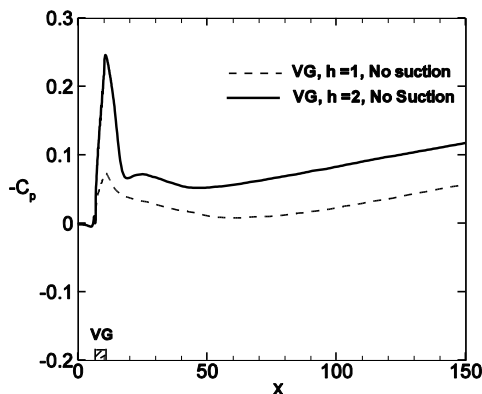


Fig. 4. Evolution of wall pressure-coefficient.

3.1.3 Mean Flow Structure

Figure 5 shows the mean streamwise velocity contours for the two cases. No separation is seen in the case *VG-1*, while two small bubbles are seen in the case *VG-2*, one of these being so tiny that its presence is hardly felt by the flow. This bubble actually sits close to the leading edge of the vortex generator blades. Figs. 6(a) and 6(b) compare the mean streamwise velocity component with the Blasius profiles while Figs. 7(a)-(d) compare the u_{rms} , u_{rms} , v_{rms} and w_{rms} respectively obtained from the two cases. In these figures, the horizontal axis is arbitrarily chosen to depict the variation in magnitude of the variables as they change their position. At all the streamwise locations shown, case *VG-2* has a fuller streamwise component of velocity near the wall signifying greater momentum transfer to wall as compared to the case *VG-1*. At $x = 12$, a streamwise location close to the trailing edge of the vortex generator, growth of perturbations can be seen. However, the magnitude of perturbations is significantly larger in the case *VG-2*, for example the maximum magnitude of u' is about 44% of the inlet free-stream velocity for the case *VG-2*, while in the case *VG-1* this is of the order of 24% only. Further, the outer layer activity is higher in case *VG-2* and it starts much earlier.

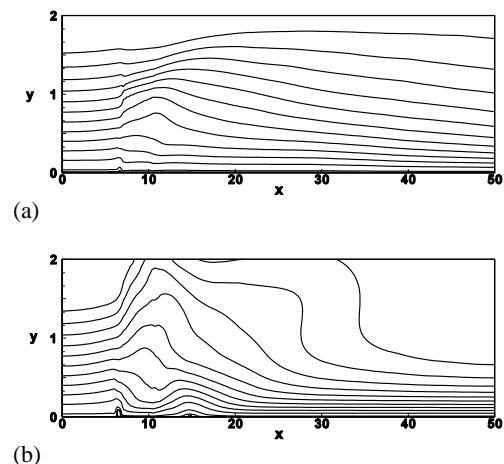


Fig. 5. Contours of mean streamwise velocity for (a) case *VG-1* and (b) *VG-2*.

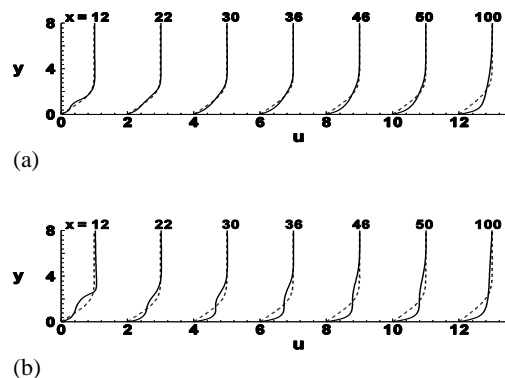


Fig. 6. Comparison of mean streamwise velocity with Blasius profiles (dashed lines) for (a) case *VG-1* and (b) *VG-2*.

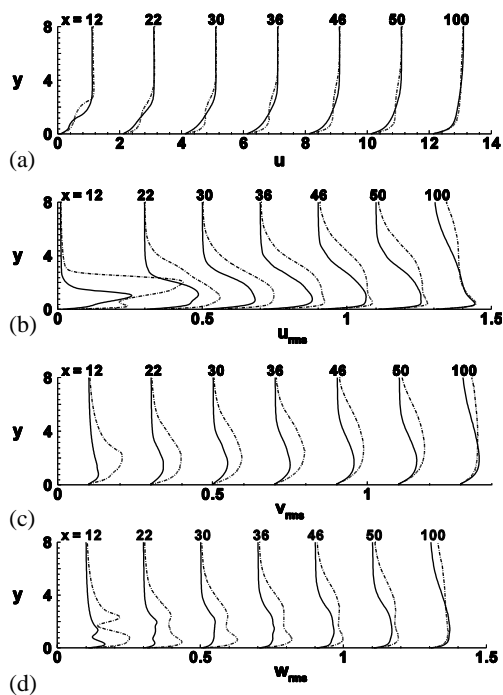


Fig. 7. Profiles of (a) u_m (b) u_{rms} (c) v_{rms} (d) w_{rms} at different streamwise locations. Solid line: case VG-1, dash-dot: case VG-2.

3.2 Time-Averaged Flow

In this section, time-averaged quantities are presented, which are not only function of x and y , but the function of z also.

3.2.1 Wall Shear-Stress

Figures 8(a) and 8(b) depict the downstream development of time-averaged wall shear stress τ_w at five spanwise locations. The locations P_1 and P_3 are close to the VG blades' trailing edges, P_2 is at the symmetry line between the two blades, P_5 is at the symmetry line between the two pairs and P_4 is in between P_3 and P_5 . It can be seen from the figures that strong three-dimensionality in shear stress is introduced by the presence of vortex generators. The wall shear stress is significantly higher in the sections close to the VG edges, especially the trailing ones

For comparison, the wall shear-stress for a laminar boundary layer (obtained from correlation for Blasius velocity profile), is also superimposed. In Fig. 8(a) it is seen that the rise in wall shear stress is much more rapid at the sections P_1 and P_3 as compared to other sections due to the strong vorticity induced by the trailing edges of vortex generators. A comparison with Fig. 8(b) shows that greater vortex generator height leads to early introduction of higher wall shear-stresses. The figures further convey the fact that the three-dimensionality introduced by the vortex generators begins to die down as the flow proceeds downstream, the decay of spanwise anisotropy being faster in the case VG-2 as the vortices rapidly spread and merge downstream of $x-x_t = 75$ whereas for VG-1 the flow remains three-dimensional till $x-x_t = 100$.

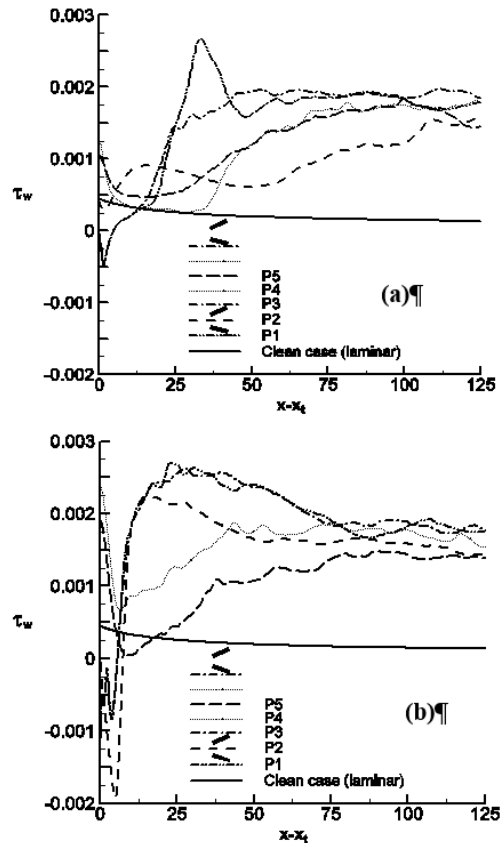


Fig. 8. Time-averaged wall shear stress at different spanwise locations for (a) case VG-1 and (b) case VG-2.

3.2.2 Velocity Field

Figures 9(a) and 9(b) show time-averaged streamwise velocity profiles at four spanwise locations for the two cases under discussion. Location 1 is between vanes of a VG, location 2 is at the symmetry-line between the two VG pairs, location 3 is exactly downstream of VG blade and location 4 is mid-way between 2 and 3. It can be immediately recognized that location 1 gives values closest to the spanwise averaged quantities while location 3 produces maximum deficit due to the rolling motion of fluid. For the case VG-2 all streamwise locations exhibit S-shaped u -velocity profiles at spanwise locations 2 and 3 indicating higher streamwise velocities near the wall and in the outer region with low values in between.

Figure 10 shows the time-averaged streamwise velocity (u) contours in the y - z plane at $x/h = 5.5, 9, 13$ and 20 for both the VG heights; the in-plane secondary velocities are also shown as vectors. At the first location ($x/h = 5.5$), which is close to the vortex generators, the shape of vortices is not completely circular but by the next location i.e. $x/h = 9$ it grows into a circle. The strong thinning effect of vortex generators on the boundary layer in the downwash region where high-momentum fluid is being transferred into the near-wall region is clearly visible. It is also seen that this effect is reduced as the vortices moves downstream.

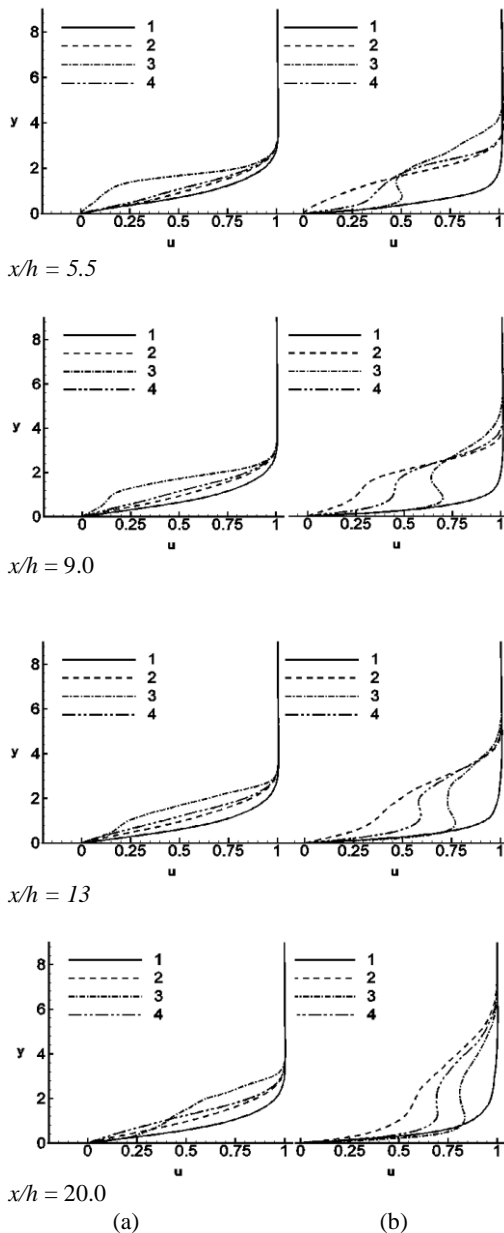


Fig. 9. Profiles of time-averaged streamwise velocity at different spanwise locations, for (a) case VG-1 and (b) VG-2.

3.2.3 Vortex Development

Identification of a vortex can be done in many ways (Jeong and Hussain, 1995). A comprehensive review of the existing techniques can be found in Jiang et al. (2004). Here, the mean streamwise

vorticity $\omega_x = \frac{\partial w}{\partial y} - \frac{\partial v}{\partial z}$ and the x -component of the

second invariant of the velocity gradient tensor

$Q_x = -\frac{\partial w}{\partial y} \frac{\partial v}{\partial z}$ have been used to identify the

vortex. As Q_x does not get any contribution from pure shear, it is considered to be a better indicator of pure rotation as compared to ω_x (Adrian et al., 2000).

The decay of generated vortices can be seen from Fig.11 showing the streamwise development of the maximum values of wall-normal velocity (v), spanwise velocity (w), streamwise vorticity ω_x and vortex strength Q_x in y - z plane. The values have been normalized with the maximum value in the most upstream plane for the respective cases. All the quantities show a decreasing trend as observed by Angele and Grewe (2007) too. For both the vortex generator cases the vorticity decays almost exponentially with axial distance due to viscous effects as reported by others too (Yao et al., 2002; Velte et al., 2007).

The decay can be approximated by $y = 1.9e^{-0.043x}$ (Fig.12) where y represents normalized streamwise vorticity in y - z plane and x is the streamwise distance. The vortices grow weaker and cover larger areas as they move downstream. The no-slip condition imposed at the wall causes strong shear which induces vorticity of opposite sign in the near-wall region. As expected, vortices generated in case VG-2 are stronger and larger in extent. The vortices move away from each other in the spanwise direction due to interaction with the image vortices. However, in the wall-normal direction the vortex centers do not show any significant upward movement as they travel downstream.

3.3 Instantaneous Flow and Three-Dimensional Structure

In this section, the development of longitudinal vortices, resultant momentum transfer and the subsequent decay of vortices are discussed. Contours of instantaneous streamwise velocity at different sections are presented for the two VG cases. The contours illustrate important features of the flow field. Figs. 13(a) and 13(b) depict contours of instantaneous streamwise velocity in two x - y planes (at $z = 7.5$ and $z = 15$) at a particular time instant for the two cases. The location $z = 7.5$ is between the two blades of vortex generator while $z = 15$ is the plane of symmetry between the two vortex generator pairs. In the case VG-1 no trace of reversed flow is seen at any of the two sections while a bubble is visible from $x = 11.0$ to $x = 18.0$ at $z = 7.5$ and the existence of a tiny bubble is seen from $x = 18.0$ to $x = 21.0$ along with a highly disturbed flow at $z = 15$ for the case VG-2 where the spanwise anisotropy created by the vortex generator of greater height is more severe as compared to the case VG-1.

Figures 14(a) and 14(b) show the top view (x - z plane) of streamwise velocity contours obtained from the two cases VG-1 and VG-2 respectively at two wall normal location ($y = 0.05$ and 0.1). In both the cases, the longitudinal vortices generated by the vortex generator tend to move in the direction in which the trailing edge points to. However, vortices generated in the case VG-1 persist for longer streamwise distance (approximately up to $x = 110$) as compared to the stronger vortices generated by the vortex generator of greater height probably due

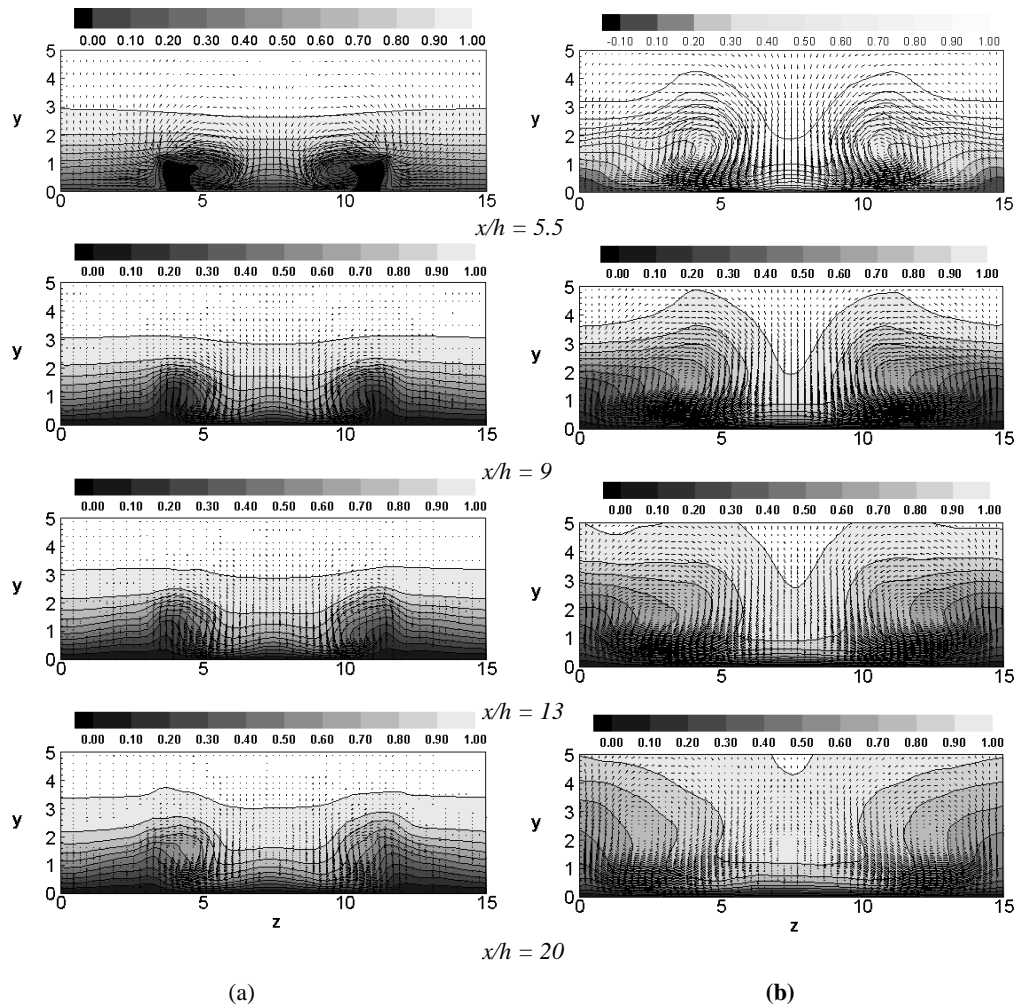


Fig. 10. Time-averaged streamwise velocity contours in y - z planes at different streamwise locations for (a) case *VG-1* and (b) case *VG-2*. Secondary flow vectors are also superimposed.

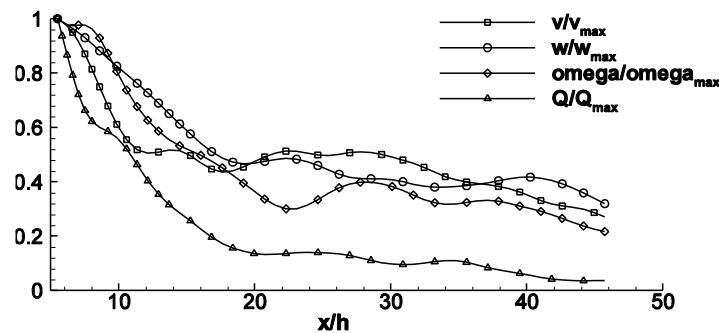


Fig. 11. Downstream evolution of normalized maximum wall-normal velocity, spanwise velocity, streamwise vorticity and vortex strength in the y - z plane.

to stronger interaction between the vortices in the case *VG-2*. This fact which is illustrated more clearly in Figs. 15(a) and 15(b) showing the side views (y - z plane) of streamwise velocity contours for four streamwise sections at the same time, is also confirmed by mean skin friction coefficient and wall shear stress distributions. In Fig. 15 location $x = 8.0$ is at a section between the leading edge and the trailing edge of the vortex generators, Location $x = 13.5$ is slightly downstream the vortex generator trailing edge.

Formation and growth of longitudinal vortices can be seen as we move downstream. In the case *VG-1* vortices can be clearly identified at $x = 20$ while the bigger and stronger vortices formed in the case *VG-2* are broken up early and individual vortices are difficult to identify at $x = 20$. In both the cases, thinning of the boundary layer in the downwash region and thickening of the upwash region are clearly seen. As expected, these effects are manifested in a more pronounced manner in the case *VG-2*.

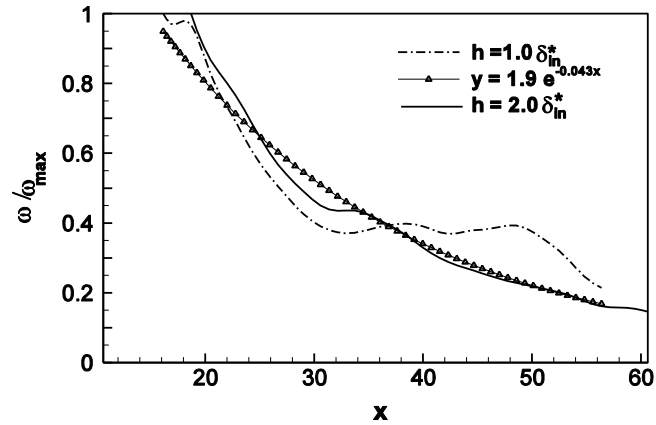


Fig. 12. Exponential decay of vorticity for the two vortex generator cases. The decay can be approximated by $y = 1.9e^{-0.043x}$ as shown.

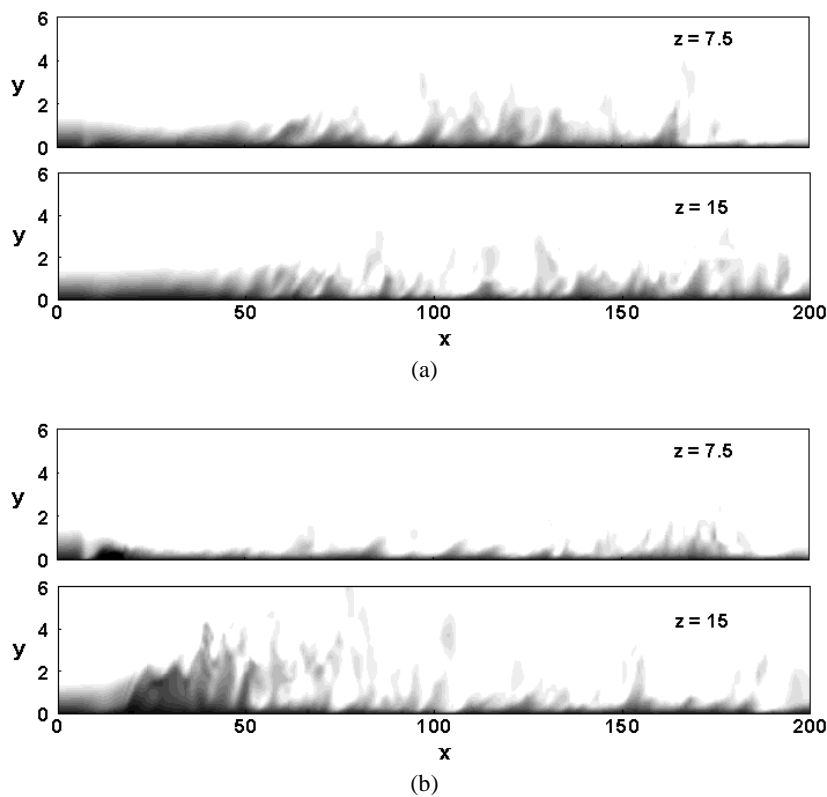


Fig. 13. Instantaneous contours of streamwise velocity in x - y planes at $z = 7.5$ and 15.0 for (a) case *VG-1* and (b) case *VG-2*. Maximum level is 0.7 , minimum level is -0.01 with 13 levels in between.

The iso-surfaces of instantaneous streamwise vorticity for the two cases are presented in Figs. 16(a) and 16(b) respectively. Figs 17(a) and 17(b) depict the iso-surfaces of spanwise vorticity. The development of longitudinal vortices downstream of vortex generators and their breakup leading to small scale structures and turbulence is clearly seen in Figs. 16-17. The figures further illustrate the fact that vortices generated in the case *VG-1* persist for longer streamwise distance as compared to the stronger vortices generated by the vortex generator of greater height probably due to stronger interaction between the vortices in the case *VG-2*.

3.4 Turbulence Statistics and Boundary-layer Relaxation

Figures 18(a) and 18(b) depict the evolution of maximum r.m.s. values of velocity fluctuations. The figures illustrate that downstream of VGs the turbulence intensity in the case *VG-1* is about 25% while in case *VG-2* it is rather high at 45%, however in both cases as the flow evolves towards homogeneous turbulence, the value of turbulence intensity decreases to about 15%.

The contours of Reynolds stresses for the cases *VG-*

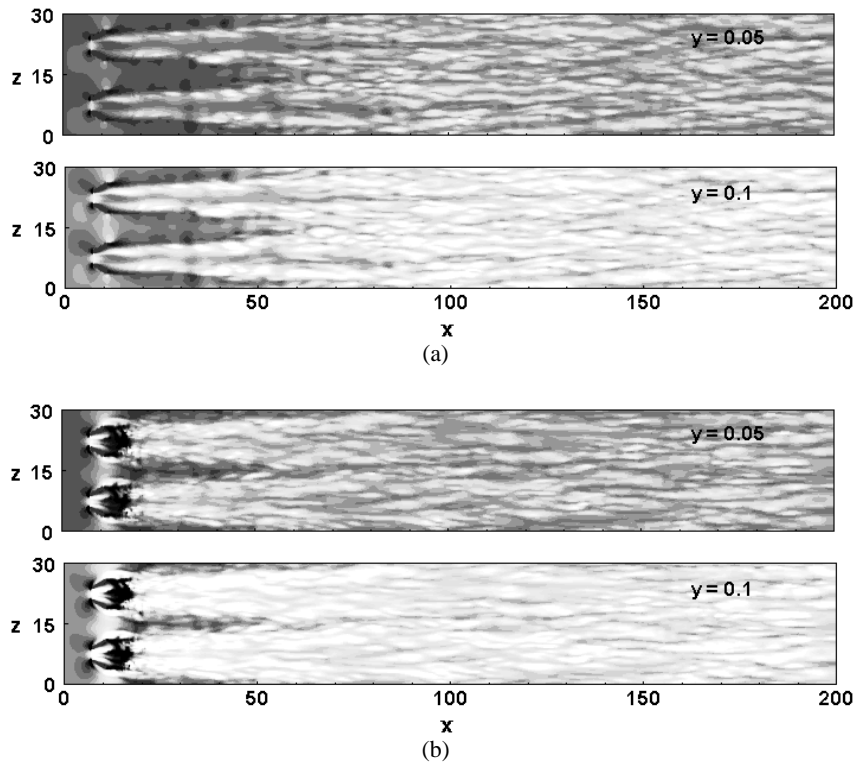


Fig. 14. Instantaneous contours of streamwise velocity in x - z planes at $y = 0.05$ and 0.1 for (a) case *VG-1* and (b) case *VG-2*. Maximum contour level is 0.23 , minimum level is -0.05 with 13 levels in between.

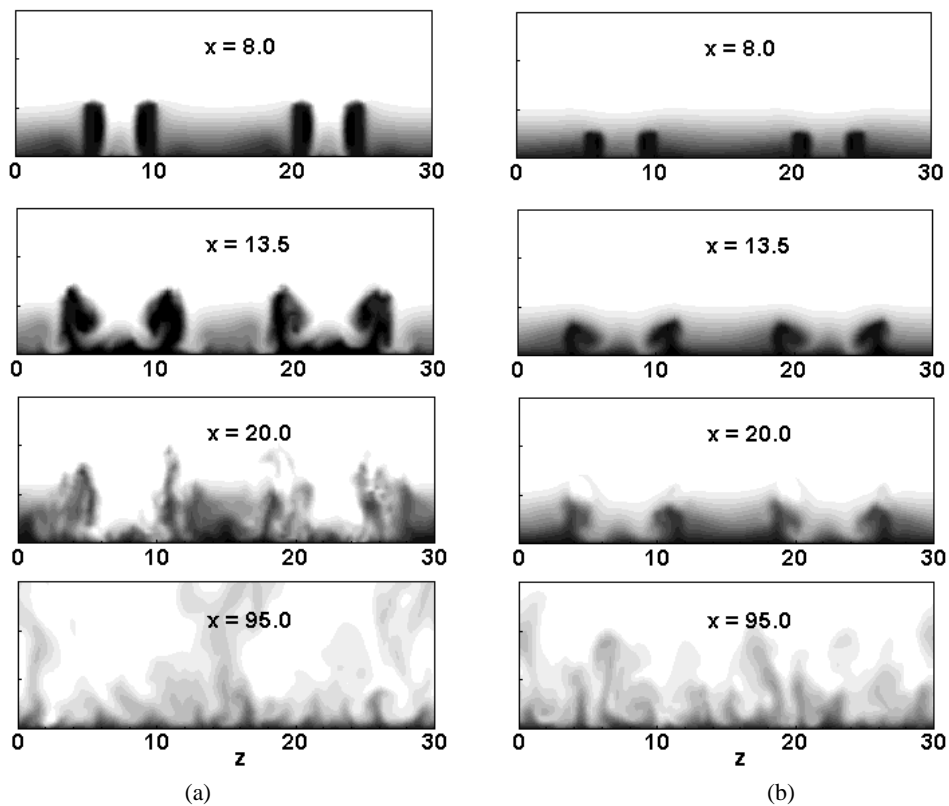


Fig. 15. Instantaneous contours of streamwise velocity in y - z planes at $x = 8.0, 13.5, 20.0,$ and 95.0 for (a) case *VG-1* and (b) case *VG-2*. Maximum level is 0.91 , minimum level is -0.002 with 13 levels in between.

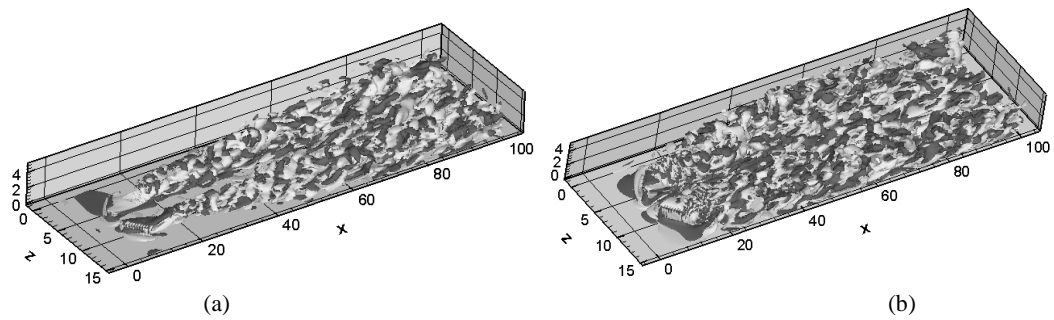


Fig. 16. Iso-surfaces of instantaneous streamwise vorticity for (a) case *VG-1* and (b) case *VG-2*. Contour levels are -0.1 and 0.1 for both the cases.

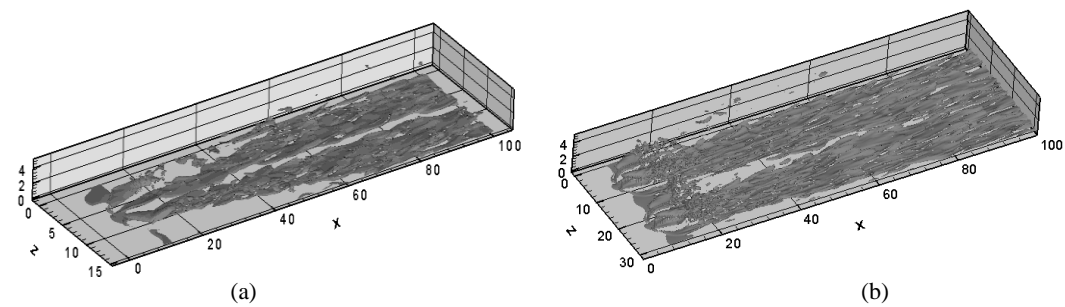


Fig. 17. Iso-surfaces of instantaneous spanwise vorticity for (a) case *VG-1*, contour level is -0.5 and (b) case *VG-2*, contour level is -0.6.

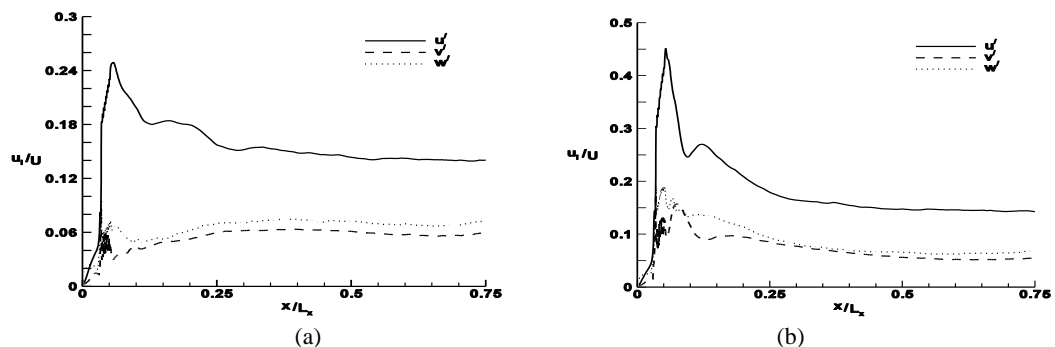


Fig. 18. Mean profiles of maximum r.m.s. values of velocity components (u' , v' , w') along the streamwise direction for (a) case *VG-1* (b) case *VG-2*.

I and *VG-2* are presented in Figs. 19(a) and 19(b) respectively. The maxima for the stresses are concentrated in the region just downstream the trailing edge of the vortex generators. However, the magnitude of stresses in the case *VG-2* is 3 to 5 times larger than that in the case *VG-1*. Contours of turbulent kinetic energy (TKE) and the production (PKE) are depicted in Figs. 20(a) and 20(b) respectively. However the magnitude of stresses in the case *VG-2* is 3 to 5 times larger than that in the case *VG-1*.

3.5 Comparison with Experimental Data

Results from the present simulations have been compared with the experimental data obtained by [Angele and Grewe \(2007\)](#) in Fig. 21. It may be noted that their vortex generator geometry and experimental conditions do not closely match those of the present simulation. The quantities v/v_{max} and

w/w_{max} closely follow the experimental observations of [Angele and Grewe \(2007\)](#) while Q/Q_{max} and ω/ω_{max} show general agreement with the trend of decay. It may be noted that the quantities without subscript, denoting their maximum value in the $y-z$ plane at a particular x -location, have been non-dimensionalized by their respective maximum values in the $y-z$ plane at $x/h = 5.5$ denoted by the subscript 'max'.

4. CONCLUSIONS

The simulations show that the IB method in conjunction with DNS can effectively simulate the time-dependent flow behind an array of passive vortex generators placed in an initially laminar boundary layer. Besides, as compared to the body-fitted grid this approach is computationally more efficient too. Investigation of instantaneous flow

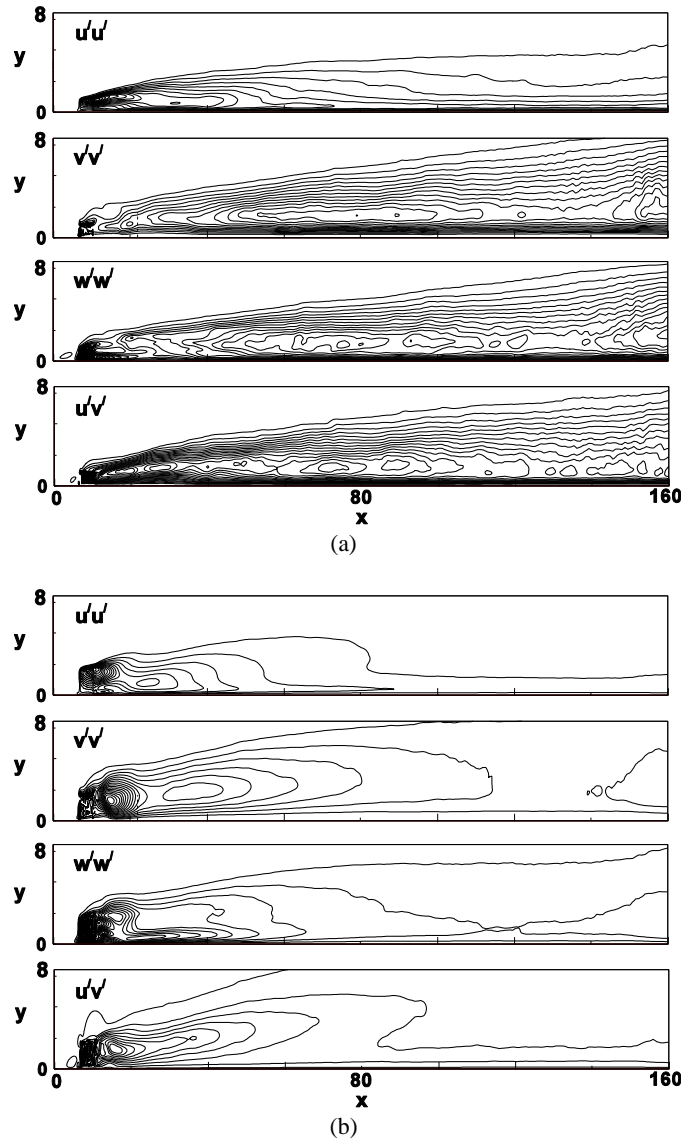


Fig. 19. Contours of fluctuation statistics, $\overline{u'u'}$, $\overline{v'v'}$, $\overline{w'w'}$ and $\overline{u'v'}$ for (a) case *VG-1*, maximum contour levels are 0.062, 0.005, 0.008 and 0.0038 respectively; (b) case *VG-2*, maximum contour levels are 0.203, 0.025, 0.035 and 0.012 respectively.

quantities at different spanwise sections aided by three-dimensional visualization confirms the high spanwise anisotropy of the flow. Production of counter-rotating streamwise vortices by the rectangular vane type vortex generators energizes the retarded near-wall flow as the helical motion of vortices bring high-momentum fluid from the outer region to wall.

It is observed from the simulations that the streamwise vortices generated by the vortex generators do not show any significant movement away from the wall in the wall-normal direction. However, in the spanwise direction the vortices move apart; their movement being along the vortex generator blade angle though this shows a diminishing trend as they travel downstream. The simulations show that vortex generators of smaller height (0.33δ) do not cause separation by their

presence and generate vortices that persist for longer streamwise distances; however the vortex generators of greater height (0.66δ) create vortices which are less persistent and their presence leads to the formation of a small separation bubble downstream. Normalized maxima of v , w , Q and ω in the y - z plane all tend to decay as we move to downstream sections. This is consistent with experimental observations. The peak vorticity decays exponentially with axial distance measured from the VG trailing-edge for which a relation has been suggested.

Just downstream of VGs, regions of highly energized turbulent patches and laminar flow are observed, illustrating high spanwise dependence which becomes homogeneous in the spanwise direction as the flow relaxes downstream becoming a canonical layer. It is seen from the evolution of

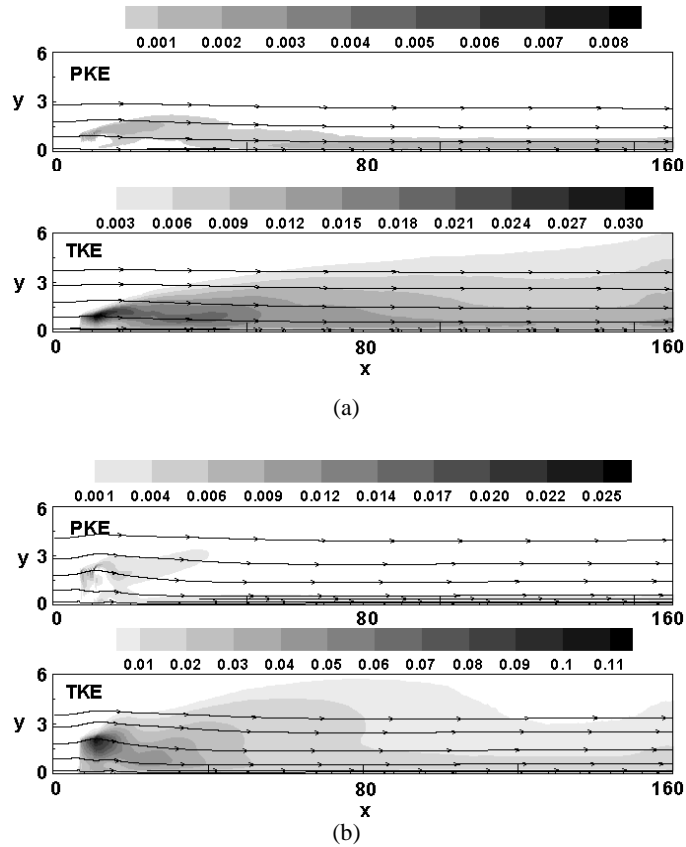


Fig. 20. Contours of mean PKE and TKE for (a) case VG-1 and (b) case VG-2.

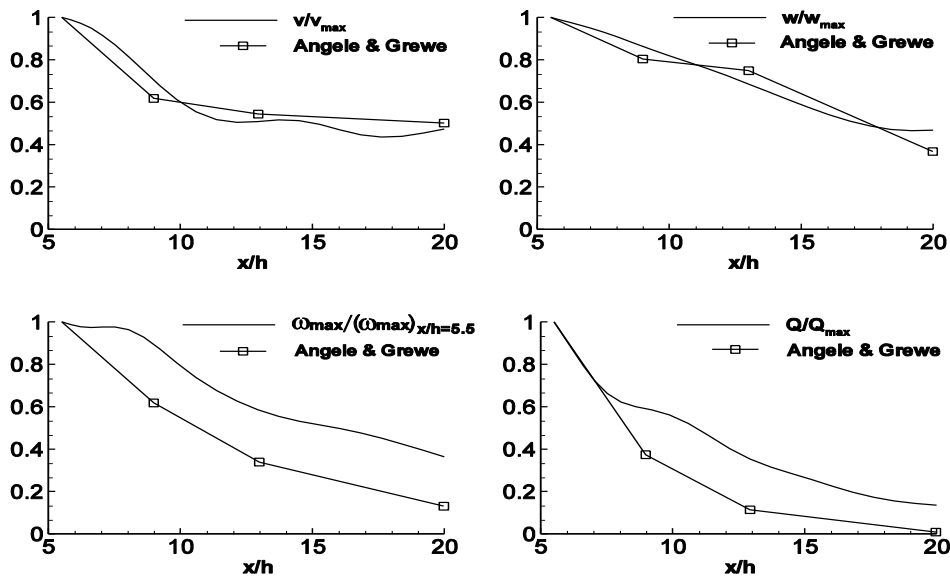


Fig. 21. Comparison of present simulation (case VG-1) with experimental data of Angele and Grewe (2007).

peak values of rms velocity fluctuations that downstream of VGs the turbulence intensity in the case VG-1 is about 25% while in case VG-2 it is rather high at 45%, however in both cases as the flow evolves towards homogeneous turbulence, the value of turbulence intensity downstream becomes about 15%.

REFERENCES

- Adrian, R. J., C. D. Meinhart and C. D. Tomkins (2000). Vortex organization in the outer region of the turbulent boundary layer. *Journal of Fluid Mechanics* 422, 1–54.

- Allan, B. G., C. S. Yao and J. C. Lin (2002). Numerical simulation of vortex generator vanes and jets on a flat plate. *1st AIAA Flow Control Conference*, St. Louis MO, AIAA paper 02-3160.
- Angele, K.P. and F. Grewe (2007). Instantaneous behaviour of streamwise vortices for turbulent boundary layer separation control. *Journal of Fluid Engineering* 129, 226-235.
- Bender, E. E., B. H. Anderson and P. J. Yagle (1999). Vortex generator modelling for Navier- Stokes codes. *Third ASME/ JSME Joint Fluids Engineering Conference*, ASME paper FEDSM99-6919.
- Bragg, M. B. and G. M. Gregorek (1987). Experimental study of airfoil performance with vortex generators. *Journal of Aircraft* 24, 303-309.
- Brown, A. C., H. F. Nawrocki and P. N. Paley (1968). Subsonic diffusers designed integrally with vortex generators. *Journal of Aircraft* 5(3), 221-229.
- Gad-el-Hak, M. and D. M. Bushnell (1991a). Separation control: Review. *ASME Journal of Fluids Engineering* 113, 5-30.
- Gad-el-Hak, M. and D. M. Bushnell (1991b). Status and outlook of flow separation control. *AIAA Paper* No. 91-0037, New York.
- Godard, G. and M. Stanislas (2006). Control of a decelerating boundary layer. Part 1: Optimization of passive vortex generators. *Aerospace Science and Technology* 10, 181-191.
- Hamstra, J. W., D. N. Miller, P. P. Truax, B. H. Anderson and B. J. Wendt (2000, August-September). Active inlet flow control technology demonstration. *ICAS-2000-6.11., 22nd International congress of the aeronautical science.*, Harrogate, UK.
- Henry, J. R., C.C. Wood and S. W. Wilbur (1956). Summary of subsonic diffuser data. *NACA RML-56F05*, Washington, DC.
- Henze, M., J. Wolfersdorf, B. Weigand, C. F. Deitz and S. O. Neumann (2011). Flow and heat transfer characteristics behind vortex generators - A benchmark dataset. *International Journal of Heat and Fluid Flow* 32, 318-328.
- Jeong, J. and F. Hussain (1995). On the identification of a vortex. *Journal of Fluid Mechanics* 285, 60-94.
- Jiang, M., R. Machiraju and D. S. Thompson (2004). Detection and Visualization of Vortices. *Visualization Handbook*. Academic Press, 287-301.
- Kerho, M., F. Hutcherson, R.F. Blackwelder and R. F. Liebeck (1993). Vortex generators used to control laminar separation bubbles. *Journal of Aircraft* 30(3), 315-319.
- Lin, J. C. and F. G. Howard (1989). Turbulent flow separation control through passive techniques. *AIAA 2nd Shear Flow Conference*, Tempe AZ, AIAA paper 89-0976.
- Lin, J. C., F.G. Howard and G. V. Selby (1990). Small submerged vortex generators for turbulent flow separation control. *AIAA Journal of Spacecraft* 27(3), 503-507.
- Lin, J.C. (2002). Review of research on low-profile vortex generators to control boundary-layer separation. *Progress in Aerospace Sciences* 38, 389-420.
- Muldoon, F. and S. Acharya (2005). Mass conservation in immersed boundary method. *Proceeds. FEDSM 2005, FEDSM-77301*.
- Orlanski, I. (1976). Simple boundary condition for unbounded hyperbolic flows. *Journal of Computational Physics* 21, 251-269.
- Pearcey, H. H. (1961). Shock induced separation and its prevention by design and boundary layer control. In G.V. Lachmann (Ed.), *Boundary Layer and flow Control, Its Principle and Applications*, Vol. 2, Pergamon press, Oxford, 1166-1344.
- Sarkar, S. and S. Sarkar (2009). Large-Eddy Simulation of Wake and Boundary Layer Interactions Behind a Circular Cylinder. *ASME Journal of Fluids Engineering* 131, 091201.
- Shan, H. (2007). Numerical simulation of flow behind active vortex generators with direct forcing immersed boundary method. *International Journal of Computational Fluid Dynamics* 21(1), 49-60.
- Shan, H., L. Jiang, C. Liu, M. Love and B. Maines (2008). Numerical study of passive and active flow separation control over a NACA0012 airfoil. *Computers and Fluids* 37, 975-992.
- Singh, N. K. and S. Sarkar (2011). DNS of a Laminar Separation Bubble. *International Journal of Mechanical and Mechatronics Engineering* 5 (9), 1757-61.
- Smith, F. T. (1994). Theoretical prediction and design for vortex generators in turbulent boundary layers. *Journal of Fluid Mechanics* 270, 91-131.
- Sohankar, A. and L. Davidson (2003). Numerical study of heat and flow in a plate-fin heat exchanger with vortex generators. In K. Hanjalic *et al.* (Ed.), *Turbulence, Heat and Mass Transfer* 4, 1155-1162, Begell House, Inc.
- Taylor, H. D. (1948a). Application of vortex generator mixing principle to diffusers. *Research Department, United Aircraft Corporation*, Concluding Report No. R-1504-5, East Hartford, CN.
- Taylor, H. D. (1948b). Design criteria for and applications of the vortex generator mixing

- principle. *Research Department, United Aircraft Corporation*, Report No. M-15038-1, East Hartford, CN.
- Velte, C. M. and M. O. L. Hansen (2013). Investigation of flow behind vortex generators by stereo particle image velocimetry on a thick airfoil near stall. *Wind Energy* 16, 775-785.
- Velte, C. M., C. Braud, S. Coudert and J. M. Foucaut (2014). Vortex generator induced flow in a high Re boundary layer. *Journal of Physics*, Conference Series 555, 012102.
- Velte, C. M., M. O. L. Hansen and K. Jønck (2007). Experimental and numerical investigation of the performance of vortex generators on separation control. *Journal of Physics*, Conference Series 75, 01230.
- Yao, C. S., J. C. Lin and B. G. Allan (2002). Flow-field measurement of device-induced embedded streamwise vortex on a flat plate. *1st AIAA Flow Control Conference*, St. Louis MO, AIAA paper 2002-3162.